ELSEVIER

Polymer 43 (2002) 7483–7491

polymer

www.elsevier.com/locate/polymer

A rheological study of concentrated aqueous nanotube dispersions

Ian A. Kinloch*, Simon A. Roberts[1], Alan H. Windle

Department of Materials Science and Metallurgy, University of Cambridge, Pembroke Street, Cambridge CB2 3QZ, UK

Abstract

The rheological behaviour of aqueously dispersed oxidised nanotubes has been studied at concentrations at which the nanotubes interacted with each other. The dispersed nanotubes represented a high aspect ratio system with a ratio of ~80. Dynamic and steady shear tests were applied to the dispersions using a cone and plate rheometer. The system was found to behave as a reversibly flocculated dispersion. The structure of the dispersions was highly strain-sensitive with the linear viscoelastic region (LVR) extending to strains of 1%. The moduli within the LVR were independent of frequency and scaled with concentration by a power law. Under steady shear the dispersions rapidly shear thinned up to a Peclet number of ~1 to 10. At higher Peclet numbers the shear thinning behaviour followed the Ostwald–de Waele power law. The dispersions were thixotropic and recovered their structure, and hence viscosity, upon standing.

Keywords: Nanotubes; Rheology; Processing

1. Introduction

Carbon nanotubes are intriguing entities with nanoscale diameters and microscale lengths, giving them large aspect ratios. Nanotubes are also stiff (Young's modulus of up to 1 TPa [1,2]) and electrically and thermally conductive [3]. Potential large-scale applications for nanotubes include electrodes, and fillers in composites. However, until recently these applications have been limited by insufficient availability of the material and difficulties in dispersing the nanotubes. Developments in the catalytic production method, by companies such as Hyperion Catalysis International (USA) and Guangzhou Yorkpoint New Energy Science and Technonlogy Development Company (China), mean that multi-walled nanotubes can now be produced in kilogram quantities on a commercial scale. However, these large-scale catalytic production methods can produce highly entangled aggregates of nanotubes. These aggregates are poorly dispersible in all solvents and controlling their dispersion is vital in the handling and processing of them.

A method to both break up the aggregates and improve the dispersivity of the nanotubes is to reflux in concentrated acid [4]. This treatment oxidises the surfaces of the nanotubes, thus facilitating their dispersion in water, other polar dispersive mediums and polymers. This treatment has provided a successful route for making poly(vinyl hydroxide)-nanotube composites [5], conducting polymer-nanotube supercapacitors [6] and nanotube films [7].

Shaffer, Fan and Windle developed this oxidation treatment for the same class of Hyperion produced nanotubes used in this work [8]. They found that the system of dispersed nanotubes had three different concentration regimes; dilute dispersion, viscoelastic gel and solid [9]. At low concentrations of nanotubes, the system behaved analogous to a dilute polymer solution. It obeyed the Schulz–Blaschke formula [10], with the viscosity of the dispersion dramatically increasing at an entanglement concentration of ~0.5 vol%. Above the entanglement concentration the system became concentrated and at ~4 vol% was capable of supporting its own weight to produce a freestanding gel. This gel was not investigated by Shaffer et al. and is studied in detail in this work. At concentrations above ~50 vol%, the dispersion formed a porous solid. They studied alignment within thin solid films of the solid formed by filtering down the dilute dispersions [8]. The films were also investigated by Li et al. who dried nanotube dispersions in a beaker under vacuum [7]. There is little other work on the rheology of nanotube dispersions, especially in the concentrated regime; although Pötschke et al. have recently investigated a nanotube-polycarbonate composite system [11].

* Corresponding author. Tel.: +44-1223-334335; fax: +44-1223-334567.

E-mail address: iak21@cus.cam.ac.uk (I.A. Kinloch).

[1] Present address: Biomaterials in Relation to Dentistry, Queen Mary, University of London, Mile End Road, London E1 4NS, UK.

0032-3861/02/$ - see front matter
PII: S0032-3861(02)00664-X

They conducted dynamic measurements and correlated them to the electrical conductivity of the composites to show the formation of a percolated network at a concentration of 0.7–1.4 vol%.

The present paper investigates the dynamic, steady and recovery behaviour of oxidised nanotubes in the concentrated regime. This regime is typical of the concentrations to be used for composite manufacture. The dispersive medium used was water, which is Newtonian, and hence simplifies the system to allow the interaction and effects of the nanotubes to be studied easily. Also, the oxidation treatment used resulted in the nanotubes being successfully dispersed in water. The results, though, can be transferred to polymer solutions or melts filled with nanotubes. The dispersions were studied rheologically using cone and plate and parallel plate geometries. Dynamic deformation studies were conducted to investigate the equilibrium, low strain rate and the recovery properties of the system. Steady shear tests were performed and models were fitted to the data obtained. The results obtained are related to possible microstructures of the dispersions.

2. Experimental section

2.1. Materials and preparation

Catalytically grown multi-walled nanotubes (Hyperion Catalysis International, cc-grade) were chemically treated as described by Shaffer et al. [8]. This treatment involved refluxing the nanotubes in a mixture of 3:1 100% sulphuric/70% nitric acid (Sigma Aldrich) for an hour. The product was then washed with distilled water to remove the acid, and resulted in a stable aqueous dispersion. The treatment shortened the nanotubes by cutting them at their defects and consuming their ends. This treatment introduced functional groups such as carbonyls and hydroxyls [12]. The treatment destroyed ~70 wt% of the initial material such that 0.5 g of material was required to make each sample for the rheology experiments.

The dilute suspensions were filtered down to a gel of the required concentration and left to rest for at least one day to allow them to relax from the forces imposed during the filtering. The weight percentage concentrations of the gels were determined by weighing a sample from each gel, drying the sample in an oven and then re-weighing it. The concentrations were converted into volume percentages by taking the density of the nanotubes to be 1.75 g cm^{-3}, as experimentally measured by Shaffer et al. [9].

2.2. Microscopy

The treated nanotubes (*primary particles*) were examined by both transmission and scanning electron microscopy (TEM and SEM). The microscopy was conducted with a Jeol 200 CX operating at 200 kV and a Jeol 640-FEG operating at 12 kV. The dimensions of the nanotubes were measured from the transmission electron micrographs using the Sicon Image analysis programme. The lengths and diameters of a total of 70 nanotubes were measured to an accuracy of 10 and 0.5 nm, respectively. The as-washed, dilute dispersions (0.1 vol%) were viewed in transmission using an optical microscope to determine if any significant secondary structure (e.g. aggregates) was present. Optical microscopy was also used to examine the effect on the secondary structure of re-diluting the concentrated dispersions or subjecting the dispersions to ultra-sonic energy.

2.3. Rheological properties

A Rheometrics Dynamic Stress SR200 rheometer was used to analyse the dispersions. A cone and plate geometry was predominantly used as this applies a homogenous shear rate across the sample (50 μm gap, 0.1 rad cone angle and 25 mm plate diameter). A parallel plate geometry (500–1350 μm gap and 25 mm diameter) was also used to ensure that the results were true to the samples since optical microscopy found small numbers of aggregates in the as-washed dispersions that were similar in size to the 50 μm gap in the cone and plate set-up. The samples were allowed to rest for 60 min after loading so that they could recover from any induced stress. (A rest period of 60 min was also used between rheological tests conducted on the same sample.) The exposed surfaces of the sample were surrounded by a light silicone oil (100 cStoke, Dow Corning) to prevent water loss during the experiments.

Measurements were taken in both dynamic and steady modes at 25 °C. Dynamic strain sweeps at a constant frequency were used to find the linear viscoelastic region (LVR) in which the storage modulus (G') and the loss modulus (G'') were independent of strain amplitude (γ_0). Dynamic frequency sweeps were conducted at constant strain within the LVR to investigate the structure of the dispersions. In these sweeps, strain was kept constant at 0.6% and the frequency varied stepwise from 0.1 to 100 rad s^{-1}. G' and G'', tan δ and the complex viscosity (η^*) were measured. (δ is the phase angle between the applied strain and the responding stress and its tangent is given by G''/G', while η^* is the maximum stress divided the oscillatory rate of the rheometer.)

Steady shear sweeps were used to investigate the flow properties of the material by recording the shear stress (σ) and viscosity (η) at increasing shear rates ($\dot{\gamma}$). The shear rate was increased in a stepwise manner, with the sample being held at each step for typically 60 s. The data obtained were scaled using the Peclet number, (Pe), which gives the relative time scales for Brownian motion of, and the hydrodynamic forces on, the particles. The Peclet number is

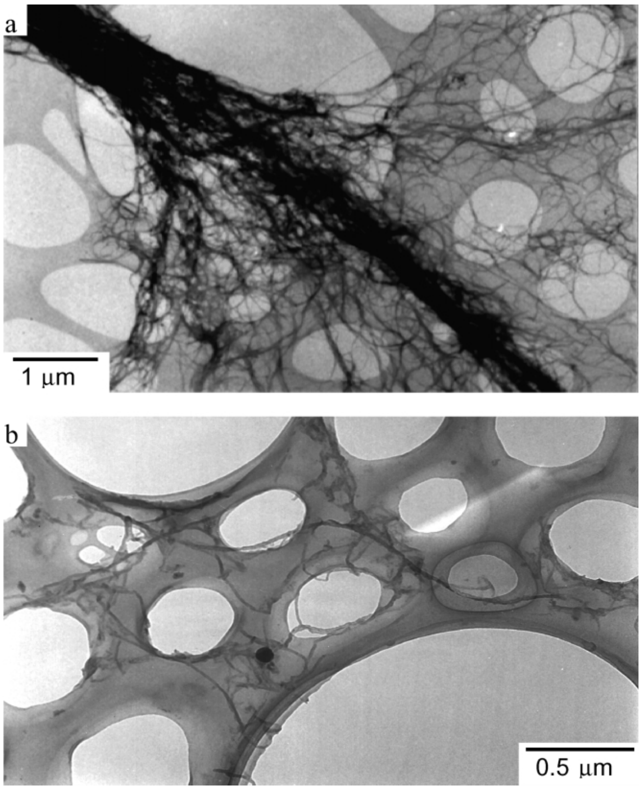

Fig. 1. (a) A TEM micrograph of a typical, as-received aggregate of nanotubes. The sample is supported on a holey carbon grid. (b) A TEM micrograph of treated nanotubes. The nanotubes are believed to have been brought together as the sample dried on the holey carbon support.

defined by:

$$Pe = \frac{\text{Timescale for Brownian motion}}{\text{Timescale for convection motion}} = \frac{\dot{\gamma}}{D_r}$$

$$= \dot{\gamma}\frac{8\pi\eta_s a^3}{3kT(\ln 2r_p - 0.5)} \quad (1)$$

where D_r is the rotary Brownian diffusion coefficient, k, Boltzman's constant, T, temperature, r_p, aspect ratio of particle, a, length of particle, and η_s is the viscosity of the solvent [13,14].

The Bingham and Herschel–Bulkley models were fitted to the flow data. These models are widely used in the industrial field for pastes, slurries and suspensions [15]. The Bingham model has a zero strain rate at stresses beneath the yield stress and acts as a Newtonian fluid above the yield stress. The Herschel–Bulkley model is an Ostwald–de Waele model with a yield stress added. The models were

Table 1
The physical dimensions of the treated nanotubes used in the present paper

	Average	Standard deviation
Length (nm)	910	650
Diameter (nm)	11	3
Aspect ratio	80	48

defined as:

$$\text{Bingham} \qquad \tau = \tau_y + \eta_\infty \dot{\gamma} \quad (2)$$

$$\text{Herschel–Buckley} \qquad \tau = \tau_y + K\dot{\gamma}^n \quad (3)$$

where η_∞ is the infinite-shear-rate viscosity, n and K, constants, and τ_y is the yield stress.

The dispersions were found to recover their properties (e.g. G', G'' and η) when the shear forces were removed. It was important to establish the timescale over which this recovery occurred. If the structure recovered instantly, the dispersions were shear-thinning, while if it occurred over a measurable time period, the dispersions were thixotropic. The recovery was investigated by conducting a series of dynamic strain sweeps on a sample and varying the rest time between the sweeps. (This method has been previously used by Pignon et al. [16]). In another experiment, samples were sheared up to rates of 1000 s^{-1} followed by the application of a dynamic stress of 1 Pa, at a rate of 10 rad s^{-1}, to record the re-building of the structure. This stress was chosen since it was sufficiently strong to measure the recovery but sufficiently weak not to completely impede the recovery.

3. Results and discussion

3.1. Primary and secondary structure in the dilute dispersions

Electron microscopy showed that the treatment had broken up the large entangled aggregates found in the as-received material, but the nanotubes retained their curved nature (Fig. 1). The dimensions of the nanotubes are given in Table 1, while the distribution of the lengths is plotted in Fig. 2. The wide variance in the physical dimensions means that the nanotubes were not an ideal system. However, recent work on substrate bound growth of carbon nanotubes will be able to produce more mono-dispersed nanotubes for future work [17,18].

The nanotubes were 20% shorter than those treated for 30 min by Shaffer et al. but the shape of the distribution remained the same [9]. This implied that during the extra treatment time used in this work only the ends of the nanotubes were attacked rather than the nanotubes being cut at defects. The rate of consumption of the nanotubes in this time was 6 nm min^{-1}.

Optical microscopy found micron-sized aggregates in all the as-washed dilute dispersions (Fig. 3a). There were more aggregates in the batches that had concentrated upon the filter as a result of infrequent stirring during filtration. (This result suggests that cross-flow filtration would reduce the aggregation, as regular reversing of the flow direction would prevent the nanotubes concentrating upon the filter.) The number and size of the aggregates also increased on ultrasonic treatment. If these difficulties were avoided, the majority of the aggregates in the dispersions were less than

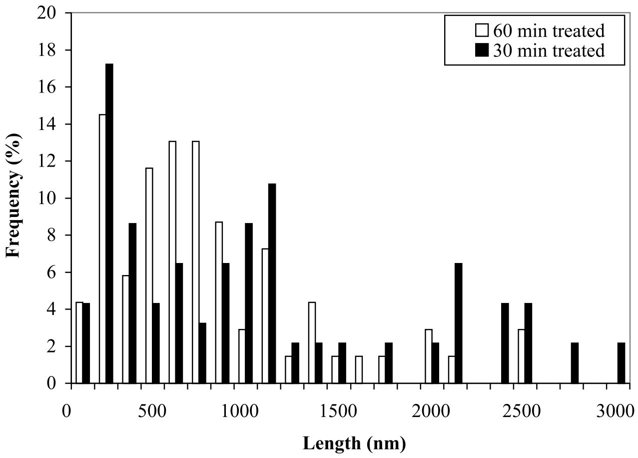

Fig. 2. The aspect ratios and lengths of the nanotubes treated for 60 min (used for the present paper) and 30 min (from Shaffer and Windle [9]). The measured lengths have been grouped into bins sized 125 nm.

10 μm in diameter. However, particles of up to 180 μm in size were observed. Despite these observations, it is believed that the majority of the nanotubes in the dilute dispersions were mainly well dispersed. The evidences for this statement were as follows:

1. When the dispersions were viewed under an optical microscope, the water surrounding the large aggregates was uniformly grey due to the well dispersed nanotubes (Fig. 3a). Dispersions of this type have been shown to be stable for up to 1 year. These well-dispersed nanotubes were smaller than the optical resolution of the microscope and therefore could not be directly observed. However upon drying as a thin layer, these dispersed nanotubes formed films in which the large aggregates were embedded (Fig. 3b).
2. Electron microscopy found individually dispersed nanotubes with the remainder clustered in groups of a few nanotubes. The clusters were probably formed as the dispersion dried during sample preparation, due to the high surface tension bringing the nanotubes together.
3. Previously, Shaffer and Windle showed that the entanglement behaviour of the dispersions could be explained using individually dispersed nanotubes [9]. Also they, and Li et al. [7], found that films produced by drying the dispersions contained local alignment of the nanotubes. This would not have been possible if the majority of the nanotubes were aggregated.

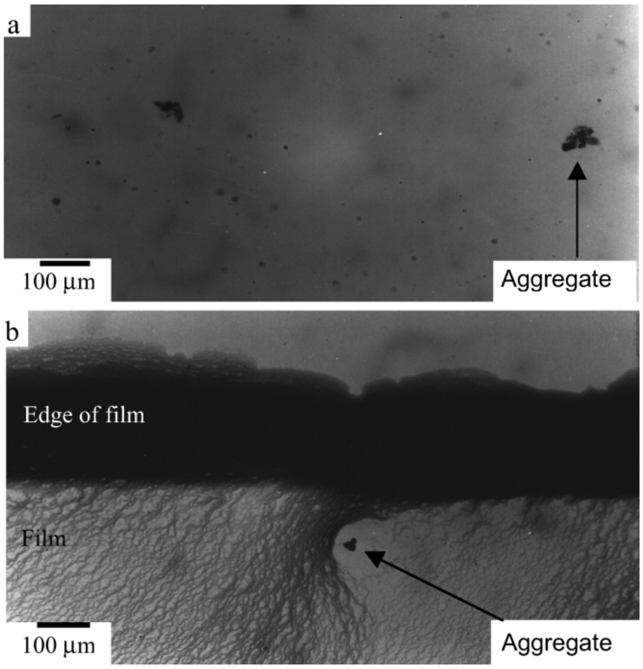

Fig. 3. (a) An optical micrograph of a typical region of an as-washed, dilute dispersion. Two large aggregates can be seen in the figure. Some of the smaller objects are bubbles in the solution. (b) An optical micrograph of a dispersion that has dried upon a glass slide to form a thin film. The large black aggregate in the centre of the image was visible before the dispersion dried, whereas the film was formed by the precipitation of the well-dispersed nanotubes during the drying process.

3.2. Observations of the concentrated dispersions

Concentrated (>0.5 vol%) dispersions appeared as viscous fluids up until ~4 vol% at which point gel behaviour became dominant and the dispersions could support their own weight as free standing gels. These gels were viscoelastic in nature and maintained their shape overnight, with a little creep at the edges. When the gels were cut both halves kept their shape. The gels absorbed, or lost water to the atmosphere, depending on the relative humidity. If the gels were squeezed, they would expel water, and when smeared a trail of dry nanotubes was left. The gel formation was partially irreversible; if the gels were dropped in excess water they rapidly broke down and dissolved back into a dilute dispersion. However, the resultant dispersion contained a greater number of aggregates than was observed in the initial dispersion prior to gel formation. The number of aggregates increased as the concentration of gel used for re-dilution increased, until 50 vol% when a solid was formed which swelled rather than re-dispersed in excess water. The solid was a brittle, three-dimensional entangled network with a very hydrophilic surface. It was found to double its mass in approximately 10 min when placed in water, with little change thereafter.

3.3. Dynamic shear properties

Dispersions with concentrations between 0.4 and 11 vol% were investigated using dynamic shear. The dispersions showed linear viscoelastic behaviour up to a critical strain of 1–2% (Fig. 4). The tests were conducted using different frequencies (1 and 10 rad s^{-1}) and with different geometries. Therefore, while it was difficult to ascertain if there was a concentration dependence on the critical strain, it was apparent that the sweeps were a true representation of the system. The

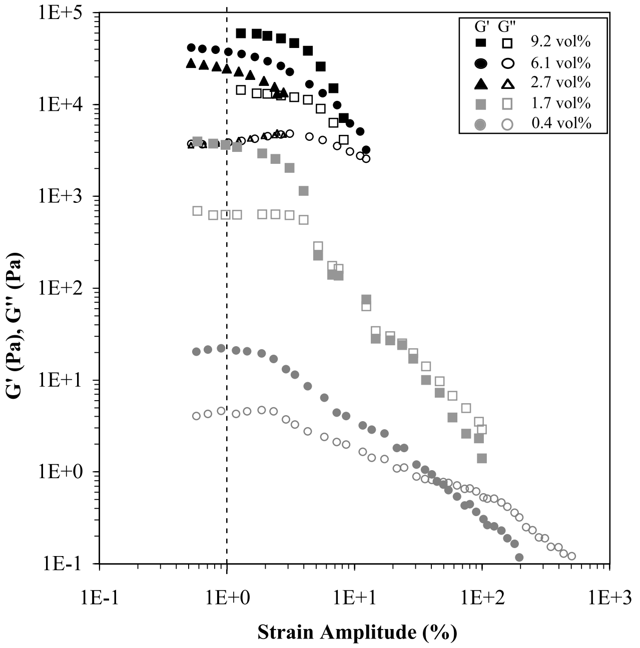

Fig. 4. Oscillatory shear measurements on the dispersions conducted at constant frequency and increasing strain amplitude (*dynamic strain sweeps*). Cone and plate geometry was used for the 6.1 and 2.7 vol% samples at 10 rad s^{-1} and used for the 0.4 vol% sample at 1 rad s^{-1}. Parallel plate geometry was used for 9.2 and 1.7 vol% samples at 10 rad s^{-1}.

structure of the dispersions rapidly broke down above the critical strain. It then entered a solid–liquid transition region, with G' and G'' crossing at ~10% strain. This type of behaviour is typical for a concentrated, reversibly flocculated network, with the values for the critical strain and the G'–G'' crossover strain being high, but not unreasonably so. (The critical strain is reported to range between 0.01 and 10%, and the crossover strain ranges between 0.5 and 15% in flocculated systems [13,19].)

Dynamic frequency sweeps were conducted within the LVR. All the sweeps found that G' and G'' were virtually independent of frequency, with G' larger than G'' and η^* decreasing with a gradient of -1 on a log–log plot (Fig. 5). The tan δ values varied from 0.1 to 0.2. The results were repeatable regardless of the starting frequency and the direction the frequency was swept in. This mechanical response for the nanotube dispersions is a classic strong gel spectrum, which is found for space-filling networks of particles. (Typical spectra and experimental data for particle networks and other types of systems can be found in Macosko [13] and Mackley et al. [20].) The G' and G'' values within the LVR were found to increase as the concentration, c, of the dispersion increased (Fig. 6). A power law was fitted to the data obtained using the cone and plate geometry. The relationships for the data were given by:

$$G' = 621c^{2.6} \text{ with the quality of fit as } R^2 = 0.97, \quad (4)$$

$$G'' = 125c^{2.4} \text{ with the quality of fit as } R^2 = 0.95. \quad (5)$$

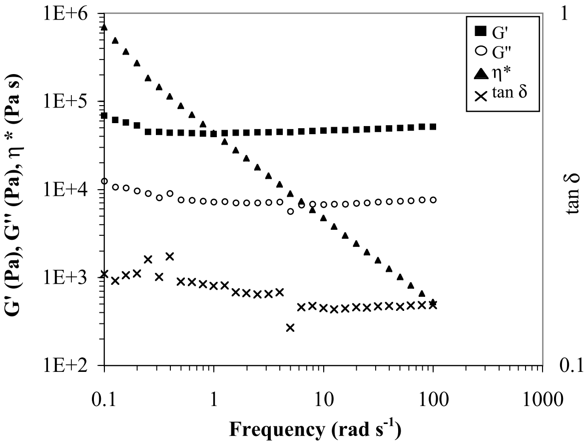

Fig. 5. A typical dynamic frequency sweep on a dispersion conducted at a strain amplitude of 0.6% (i.e. within the LVR, see Fig. 4). This spectrum is typical of a 'strong gel'. (9.2 vol% dispersion analysed using a parallel plate geometry).

Power law relationships have also been found experimentally in other percolated networks with the value of index varying between 2.5 and 4.1 [13].

The parallel plate geometry was used to confirm that the aggregates were not acting as bridging particles between the cone and plate, as previously discussed. Fig. 6 shows that there was no significant difference between the results obtained from the different measuring geometries, taking experimental scatter into account. This was expected as only a very small portion of the sample used in the cone and plate experiments had a thickness comparable to the small number of large aggregates observed.

3.4. Steady shear properties

The results for the flow behaviour of the dispersions are

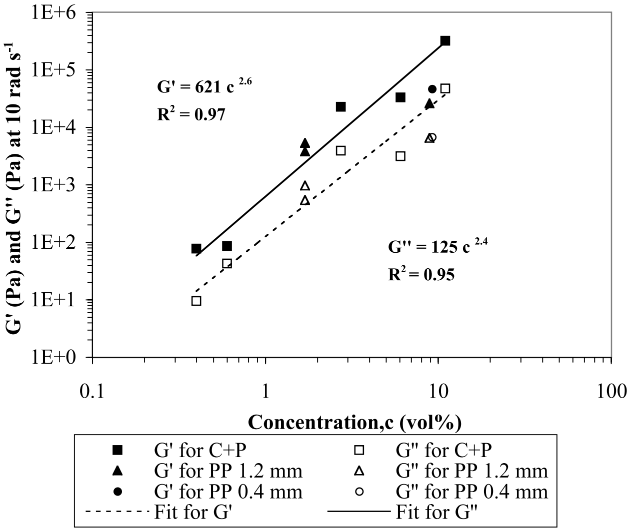

Fig. 6. G' and G'' within the LVR at a frequency of 10 rad s^{-1} as a function of concentration. The graph shows data for both cone and plate (C + P) and parallel plate (PP) geometries. Only the C + P data are used in the power law fits.

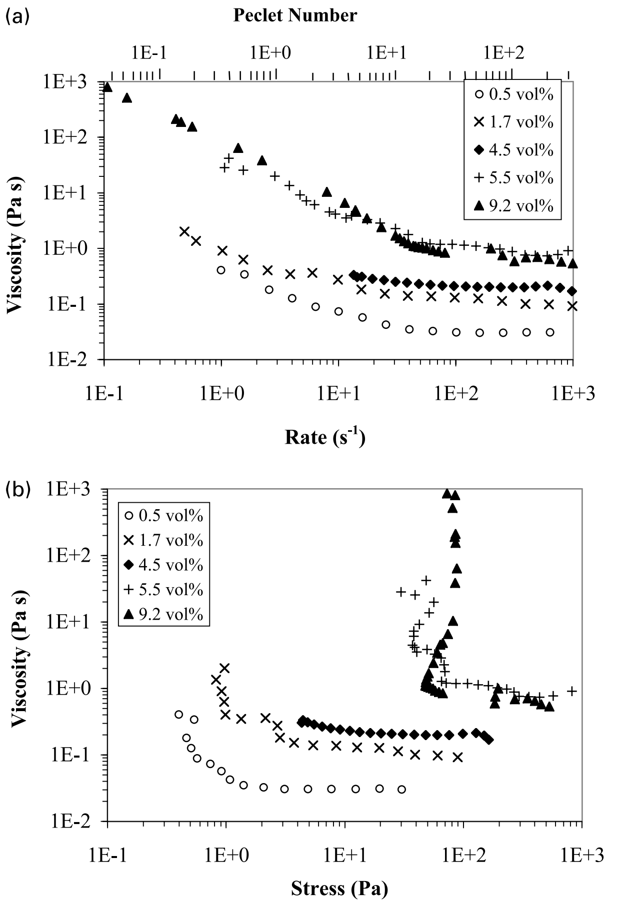

Fig. 7. Steady shear rate flow behaviour of the dispersions (4.5 and 5.5 vol% were conducted using a cone and plate geometry, while the others were conducted using a parallel plate geometry).

shown in Figs. 7 and 8. The data were scaled by using the Peclet number, as given in Eq. (1):

$$Pe = \dot{\gamma}\frac{8\pi 0.001 \times (910 \times 10^{-9})^3}{3k300((\ln 2 \times 80) - 0.5)} = 0.33\dot{\gamma} \qquad (6)$$

(The data used were: $T = 300$ K, $a = 910 \times 10^{-9}$ m, $r_p = 80$, $\eta_s = 0.001$ Pa s and $k = 1.38 \times 10^{-23}$ J K^{-1}).

The result of inserting these data was that the *Pe* was equivalent to multiplying the shear rate by 0.33. The dispersions significantly shear thinned and their behaviour could be characterised into two regions depending on *Pe*: Region 1 from low *Pe* to ~ 5 and Region 2 at $Pe > 5$ (these regions are clearer in Fig. 8). In the first region, the viscosity decreased by up to three decades while the stress remained approximately constant (Fig. 7b). For the experimental data this was effectively a yield stress with its values ranging from 1 to 80 Pa, depending on the concentration. However, it is believed not to be a true yield stress, but rather a thixiotropic region observed due to changes in the microstructure, as discussed later. It is expected that on a sensitive, strain controlled rheometer, this shear thinning region would tend to a Newtonian plateau at lower shear

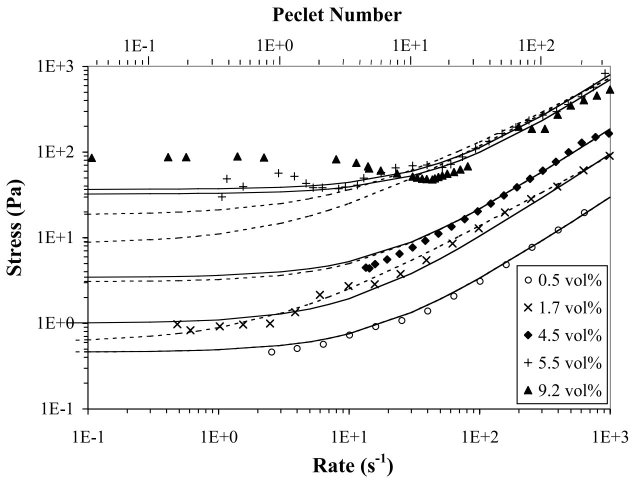

Fig. 8. The fit of the models to the steady shear rate flow data. (The solid lines show the fit of the Bingham model and the dashed lines show the fit of the Herschel–Buckley model.)

rates, as described by Aerschot and Mewis for reversibly flocculated silica particles [21,22].

In Region 2 the stress increased with increasing shear rate. This transition occurred at a Peclet number of 1–10, depending on the concentration, and therefore corresponded to when the hydrodynamic forces on the particles started to dominate over their Brownian motion (higher concentration dispersions entered Region 2 at higher shear rates.) The Ostwald–de Waele, or power law, model described the shear stress within this region with an average $n = 0.89 \pm 0.10$.

Table 2 gives the constants and the χ^2 quality of fit values obtained when the Bingham and Herschel–Bulkley models were applied to the experimental data. The fits are also plotted with the shear data in Fig. 8. The Herschel–Bulkley model should have fitted the data the best due to it being a combination of yield stress at low *Pe* (i.e. Region 1 in the data) and a power law model at higher *Pe* (i.e. Region 2). However, while the model did fit the data well for low concentration dispersions, it was not able to fit the experimentally observed sharp transition from yield stress to power law behaviour at higher concentrations. (Fitting to equally spaced data points does not significantly improve the fit.) The Bingham model was a better fit for these higher concentration dispersions due to its prediction of a sharper transition from yield stress to Newtonian behaviour. (The Bingham model is effectively the Herschel–Bulkley model with $n = 1$, so should have only fitted those curves with $n \sim 1$, such as 0.5 vol%.)

3.5. Cox–Merz rule

The nanotube dispersions were found not to obey the Cox–Merz rule (Fig. 9). This rule is an empirical observation which states that the steady shear rate viscosity and the complex viscosity are closely super-imposable for numerically equivalent values of shear rate and frequency

Table 2
The constants and quality of fit for the Bingham model and Herschel–Bulkley models to the steady shear data (Fig. 8)

Concentration of nanotubes (vol%)	Bingham model			Herschel–Bulkley model			
	Yield stress τ_y (Pa)	Viscosity η_∞ (Pa s)	Quality of fit χ^2	Yield stress τ_y (Pa)	n	K	Quality of fit χ^2
0.5	0.5	0.30	1.0	0.5	1.01	0.03	1.0
1.7	1.0	0.03	2.1	0.6	0.84	0.28	1.3
4.5	3.4	0.19	1.5	3.0	0.98	0.20	1.3
5.5	36.5	0.76	1.5	18.0	0.80	2.81	2.7
9.2	32.3	0.66	3.6	8.5	0.82	2.50	5.3

[23]. The advantage of the rule is that it allows steady shear viscosity to be predicted from dynamic data and vice versa. However, the rule only holds for isotropic polymeric solutions and polymer melts (i.e. not to liquid crystals or flocculated systems). Therefore, since it cannot be applied to the data present here, it confirms the fact that the nanotubes are interacting and behaving as a concentrated dispersion. Also, it means that the processing behaviour of the nanotubes cannot be elucidated directly from dynamic tests.

3.6. Recovery behaviour

The results of four dynamic strain sweeps conducted on the same sample of an 8.9 vol% dispersion, are given in Fig. 10. These experiments were conducted to assess the recovery period of the dispersions and evaluate if there was any permanent damage to their structure. The sample underwent dynamic strain sweeps from 0.6 to 40% at a frequency of 10 rad s^{-1} with each sweep taking 5 min. The sample was left for different periods of rest between each sweep with the rest times being 67, 30, 0.5 and 70 min, given in the order used after the initial sweep. The G' moduli at 40% strain were the same for all the experiments. This shows that the structure was broken to a similar state, regardless of shear history. It took between 30 and 70 min for the moduli to recover their initial values, meaning that the dispersions were thixotropic. However, it can be seen that the original structure was never fully recovered since the G'' values were higher than those observed in the initial structure. Also, both G' and G'' decreased more rapidly with strain after the first sweep had been conducted. Therefore, the recovered structure was more viscous and strain sensitive than the initial structure. It was found that the recovered dispersions retained their strong gel nature.

The steady shear rate sweeps broke down the structure of the samples more severely than the dynamic strain sweeps. Fig. 11 shows the recovery of a 4.5 vol% dispersion after a

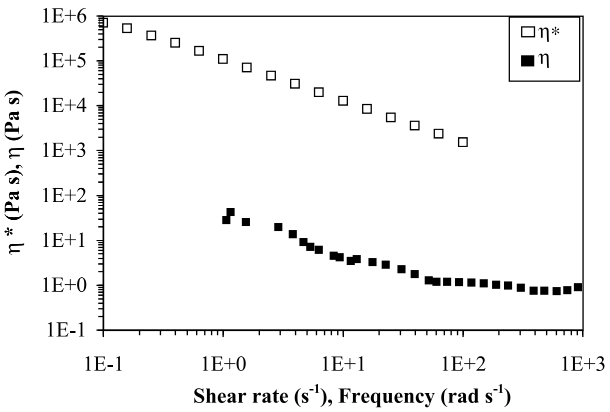

Fig. 9. Comparison of the complex and steady shear viscosities of a 5.5 vol% dispersion. The two viscosities would be closely super-imposable if the Cox–Merz rule was obeyed.

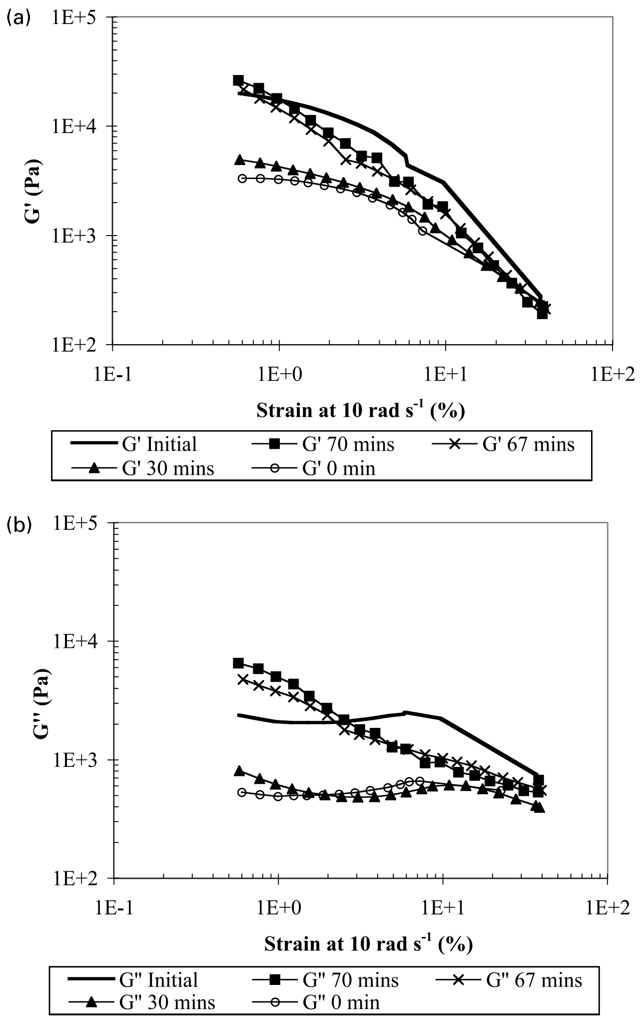

Fig. 10. Dynamic strain sweeps conducted on an 8.9 vol% dispersion with different rest periods between each sweep. The data is split across two graphs for clarity. The order of the experiments is given in the text.

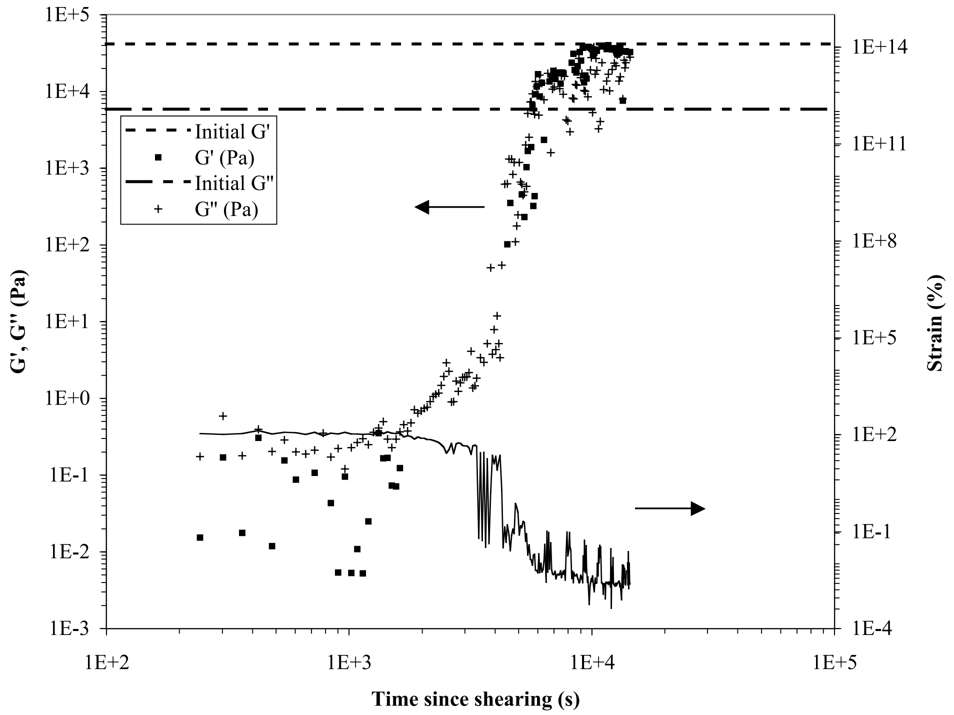

Fig. 11. Recovery of a 4.5 vol% dispersion after it had been sheared in a steady shear rate sweep from 1 to 1000 s^{-1}. The recovery was observed by applying a dynamic 1 Pa stress at a frequency of 10 rad s^{-1} to the sample.

steady shear rate sweep of 1–1000 s^{-1} with a total of 30 steps, shearing for 20 s per step. The recovery was measured using a probing stress of 1 Pa at 10 rad s^{-1}. G' and G'' were observed to recover to their pre-shear values within 1.5 h. The recovery was not steady; initially there was a slow increase in the moduli with time. This was followed by a dramatic increase in the moduli, after which point the moduli tended towards their initial values. (The fact that it tends to its initial values shows that a sufficiently long rest period was used between loading and testing samples.)

An alterative method to view the recovery data is to observe the strain produced by the 1 Pa stress. An hour into the recovery period the strain decreased from 27 to 0.05%, showing the structure reforming.

The structure of the dispersions, however, did not always recover from high strains and could be destroyed by the tests. The shear rate tests were most liable to destroy the samples when rates above 1000 s^{-1} were applied.

3.7. Discussion of the microstructure

The concentrated carbon nanotube dispersions acted as reversibly flocculated networks, as discussed above. The microstructure of the dispersions would therefore be similar to that of other flocculated networks. Hence, at rest, the nanotubes formed a spacing-filling network with the electrostatic forces between the nanotubes providing the observed elastic behaviour at very low strain rates. This network would give the electrical conductivity in nanotube composites, as observed by Pötschke et al. [11] At very low strain rates ($Pe \ll 1$) the network would creep with the majority remaining intact, and it reforming as quickly as it is broken. The network breaks down at strain rates outside the LVR, which causes the viscosity and moduli of the system to decrease rapidly with increasing rate. The apparent yield stress observed in the experimental data occurred in this region. A plausible explanation for this 'yield stress' was proposed for flocculated networks by Barnes [24]. He argued that under shear the network broke down into floccs. The size of the floccs depends on the ratio of the Brownian motion, which forms the floccs, and the shear forces which break the floccs apart. (This ratio is effectively the Peclet number.) This ratio gives an equilibrium flocc size for each shear rate, with the flocc size decreasing with increasing shear rate. Therefore as the rate is increased, the floccs break into smaller floccs, which require less stress to flow, keeping the stress virtually constant with increasing shear rate. At a sufficiently high shear rate the floccs break up into the primary particles and then the stress climbs with increasing rate. The Barnes explanation appears appropriate for the nanotube dispersions since the deviation from the yield stress occurred when the shear forces were dominating, i.e. $Pe = 1–10$.

At the higher shear rates the nanotubes would be fully dispersed. Based upon the re-dispersion work this corresponds to the majority of the nanotubes being individually dispersed and the remainder existing as small agglomerates. It is expected that the nanotubes aligned with the shear flow in the final stage. (Alignment of the nanotubes would explain the shear-thinning present at high shear rates.) Shear alignment of the nanotubes is supported by the work of Kumar et al., who found that nanofibres aligned near the surface of an extruded, and subsequently drawn, polypropylene fibre [25]. The hypothesis is also supported by the shear alignment of other asymmetric particles in concentrated systems (e.g. kaolinite in water shear aligns [26]).

4. Conclusions

Catalytically grown nanotubes were oxidised and dispersed in water. Some micron-sized aggregates were found within the as-washed dispersions but it was concluded that the majority of the nanotubes were well dispersed. The number of aggregates was found to increase as the concentration of the dispersions was increased. At concentrations of 50 vol% and greater the dispersions could not be re-diluted.

The dispersions were very strain sensitive with the LVR extending to strains of $\sim 1\%$. Within the LVR the dispersions had a strong gel mechanical spectrum. G' and G'' were found to scale with a power law with respect to concentration Under steady shear the dispersions rapidly shear thinned, with an apparent yield stress up to a Peclet number of ~ 1. At higher Peclet numbers the dispersions shear thinned more gradually as described by a power law model with an average index of 0.86. The Bingham model described the experimental steady shear flow data better than the Herschel–Bulkley model. The dispersions were thixotropic and recovered their structure upon rest with recovery mainly occurring after 60 min. The behaviour of the dispersions is that of a reversibly flocculated dispersion and the microstructure of the nanotubes was discussed based upon the literature of other flocculated systems. It is interesting to note that this behaviour indicates a transition from polymer solution [10] to particle dispersion properties as the nanotube concentration was increased from the dilute to the concentrated regime.

Acknowledgements

The authors are grateful to Prof. Malcolm Mackley (Department of Chemical Engineering, University of Cambridge) for helpful discussions, the EPSRC for funding and Hyperion Catalysis International, Cambridge, USA for supplying the nanotubes.

References

[1] Yu M-F, Files BS, Arepalli S, Ruoff RS. Phys Rev Lett 2000;84: 5552–5.
[2] Yu M-F, Lourie O, Dyer MJ, Moloni K, Kelly TF, Ruoff RS. Science 2000;287:637–40.
[3] Harris PJ. Carbon nanotubes and related structures: new materials for the 21st century. Cambridge: University Press; 1999.
[4] Esumi K, Ishigami A, Nakajima A, Sawada K, Honda H. Carbon 1996;34:279.
[5] Shaffer MSP, Windle AH. Adv Mater 1999;11:937–41.
[6] Hughes M, Chen GZ, Shaffer MSP, Fray DJ, Windle AH. Chem Mater 2002;14:1610–16137.
[7] Li Y-H, Xu C, Wei B, Zhang X, Zheng M, Wu D, Ajayan PM. Chem Mater 2002;14(2):483–4858.
[8] Shaffer MSP, Fan X, Windle AH. Carbon 1998;36:1603–12.
[9] Shaffer MSP, Fan X, Windle AH. Macromolecules 1999;32:6864–6.
[10] Schulz GW, Blaschke FJ. Prakt Chem 1941;158:130.
[11] Pötschke P, Fornes TGD, Paul DR. Polymer 2002;43:3247–55.
[12] Shaffer MSP. PhD thesis, University of Cambridge; 1999.
[13] Mewis J. In: Macosko MW, editor. Rheology: principles, measurements and applications. New York: Wiley–VCH Inc; 1993.
[14] Russel WB, Saville DA, Schowalter WR. Colloidal dispersions. Cambridge: University Press; 1991.
[15] Lapasin R, Pricl S. Rheology of industrial polysaccharides: theory and applications. London: Chapman & Hall; 1995.
[16] Pignon F, Magnin A, Piau J-M, Cabane B, Lindner P, Diat O. Phys Rev E 1997;56:3281–9.
[17] Singh C, Shaffer M, Kinloch I, Windle A. Physica B 2002;323: 339–40.
[18] Andrews R, Jacques D, Rao AM, Derbyshire F, Qian D, Fan X, Dickey EC, Chen J. Chem Phys Lett 1999;303:467–74.
[19] Shih WY, Shih WH, Aksay IA. J Am Ceram Soc 1999;82:616–24.
[20] Mackley MR, Marshall RTJ, Smeulders JBAF, Zhoa FD. Chem Engng Sci 1994;49:2551–65.
[21] van der Aerschot E, Mewis J. Colloids Surf 1992;69:15–22.
[22] Barnes HA, Walters K. Rheol Acta 1985;24:323–6.
[23] Cox WP, Merz EH. J Polym Sci 1958;28:619–22.
[24] Barnes HA. J Non-Newtonian Fluid Mech 1997;70:1–33.
[25] Kumar S, Doshi H, Srinivasarao M, Park JO, Schiraldi DA. Polymer 2002;43:1701–3.
[26] Brown ABD, Clarke SM, Convert P, Rennie AR. J Rheol 2000;44: 221–33.